International Journal of Thermophysics, Vol. 21, No. 1, 2000

Transient Hot Strip (THS) Method: Uncertainty Assessment

U. Hammerschmidt[1, 2] and W. Sabuga[1]

Received March 17, 1999

The transient hot strip (THS) method can be used to measure simultaneously the thermal conductivity λ and diffusivity a of dielectrics within a few minutes. However, although the method has been known for 20 years, there is no complete assessment of its uncertainty. First, the underlying complex mathematical model makes any error analysis a tedious and complicated task. Secondly, the *ISO Guide to the Expression of Uncertainty in Measurement* does not apply directly because of the classical model's implicit character. In the present paper, the combined standard uncertainty u of the THS method has been determined by applying two different models. First, we start from the classical nonlinear model. The major sources of errors are analyzed, namely, the ideal model errors, the evaluation errors, and the measurement errors. Next, a newly developed numerical procedure combines all the components in a way that the resultant standard uncertainties of the nonlinear model, $u(\lambda)/\lambda = 2.6\,\%$ and $u(a)/a = 11\,\%$, comply as closely as possible with the principles of the ISO Guide. Second, we start from the recently presented linear expression of the THS mathematical model that is briefly discussed. Since this approximation is explicit in both measurands, the uncertainties, $u(\lambda)/\lambda = 2.5\,\%$ and $u(a)/a = 11\,\%$, are determined in full accordance with the ISO guide. The uncertainty in thermal conductivity is experimentally assessed against the standard reference CRM 039 (Pyrex). The results obtained are in excellent agreement with the theoretical values.

KEY WORDS: linear working equation; nonlinear working equation; standard uncertainty; thermal conductivity; thermal diffusivity; transient hot strip method.

1. INTRODUCTION

In a transient hot strip (THS) setup a thin metal strip serves as the active sensor to measure the thermal conductivity λ and thermal diffusivity a of

[1] Physikalisch-Technische Bundesanstalt, Bundesallee 100, D-38116 Braunschweig, Germany.
[2] To whom correspondence should be addressed.

0195-928X/00/0100-0217$18.00/0

a dielectric. Clamped between the brick-shaped sample halves, the resistive heated strip's temperature rise in time, $\Delta T(t)$, can easily be monitored as its voltage drop $\Delta U(T(t))$. This THS signal provides a measure of λ and a within a few minutes. So far, for both measurands there is no uncertainty assessment according to the ISO *Guide to the Expression of Uncertainty in Measurement* [1]. In Ref. 1 an explicit mathematical model is presumed as the basis for the analytical treatment.

The THS signal is governed by Gustafsson's working equation [2]. Given in terms of the nondimensional time τ, it is nonlinear and implicit. Thus, the measurands cannot be derived analytically; rather, they have to be estimated (e.g., Ref. 3). Moreover, the working equation is practically valid only piecewise within an undefined interval of time. This interval can be located by trial and error only. Besides this severe "model error," there is an "evaluation error" arising from the nonlinear parameter estimation, and, finally, any observed THS signal is itself subject to "measurement errors."

We analyze all three types of the above major errors in order to estimate the uncertainty of what is referred to by us as the nonlinear THS method. For this first of two assessments of this work we had to derive a new nonlinear uncertainty estimator for implicit models since the mathematical character of the related working equation does not allow a complete analytical treatment as given by ISO. The procedure follows as closely as possible the recommendations of the ISO Guide. It focuses not on an analytical but on a numerical estimation of the variances of both the measurands and is presented here for the first time. Within the framework of the error analysis, we also quantify the sensitivity of λ and a to errors in the measurement inputs.

As mentioned above, the classical model leads to a complex signal analysis that may yield unreliable results for the measurands. As recently presented in Ref. 4, considerable improvement can be achieved by an approximation of the fundamental working equation. Because of its asymptotic behavior, this equation can be (quasi)linearized in terms of $\ln t$, the natural logarithm of real time. As in the case of the closely related transient hot wire (THW) method (e.g., Ref. 5), a THS signal no longer inclines entirely nonlinearly if plotted against $\ln t$. There is a line segment, expressed as $\Delta U(t) = m \ln t + n$, that not only yields explicitly both measurands $\lambda = \lambda(m)$ and $a = a(m, n)$, but also provides additional information on the model's time domain validity in practice. Here, this procedure is referred to as linear THS method.

The new linear evaluation technique is still based upon the classical theoretical model and the fundamental experimental setup. Therefore, the potential sources of model and measurement errors continue to exist.

Nevertheless, the resulting standard uncertainty may vary from that of the nonlinear method since linearization itself causes errors. Due to the linear and explicit character of the new working equation, we were able to estimate the uncertainty in full agreement with the ISO guide.

The results obtained here for both signal analysis methods are experimentally assessed against the standard reference CRM 039 (Pyrex).

2. THEORY

The mathematical procedure in this work starts in Section 2.1 with a brief overview of the classical physical model along with its nonlinear solution obtained by Gustafsson et al. [2]. The underlying ideal assumptions imply two major model errors for practical purposes that are discussed first. Then, the evaluation errors introduced by the nonlinear data analysis are analyzed. In Section 2.2, first, the linearization of the working equation is outlined briefly. The complete treatment is presented at some length in Ref. 4. Second, the associated linearized model errors are analyzed. Finally, we discuss the linear evaluation errors.

2.1. Ideal Model

A two-dimensional metal strip ($x=0,\ -d<y<+d,\ -\infty<z<\infty$) of width $D=2d$ is entirely surrounded by an unbounded homogeneous and isotropic dielectric, initially at a temperature $T(x, y, z, t=0)=T_0$. When a constant electric current I is passed through the strip, it simultaneously serves as a continuous heat source of rate $\Phi=UI$ and as a resistance thermometer of output voltage $U(T(t))$. This transient THS signal $U(T(t))$ provides a measure of the dielectric's thermal conductivity λ and diffusivity a. It is specified by the strip source solution of Gustafsson et al. [2]:

$$\Delta U(T(t))=U(T(t))-U_0=\frac{\alpha U_0^2 I}{2\sqrt{\pi}\,L\lambda}\,f(\tau)=kf(\tau) \tag{1}$$

where

$$f(\tau)=\tau\,\mathrm{erf}(\tau^{-1})-\frac{\tau^2}{\sqrt{4\pi}}\left[1-\exp(-\tau^{-2})\right]-\frac{1}{\sqrt{4\pi}}\,\mathrm{Ei}(-\tau^{-2}) \tag{2}$$

$$k(\lambda)=\frac{\alpha U_0 \Phi}{2\sqrt{\pi}\,L\lambda} \tag{3}$$

and

$$\tau = \frac{\sqrt{4at}}{D} \tag{4}$$

Here U_0 denotes the voltage drop at $t = 0$, and α the temperature coefficient of the electrical resistance of the strip of length $L \gg D$.

In practice, a THS signal $U(t)$ is monitored pointwise as the time series of N ordered pairs $U(t_i) = U(t_0)$, $U(t_1)$, $U(t_2)$, ..., $U(t_N)$. By evaluation of the amplitude $k(\lambda)$ and shape $f(\tau(a))$ of this signal, the thermal conductivity λ and the thermal diffusivity a of a finite sample can be derived, in principle. However, the working equation [Eq. (1)] suffers from three essential drawbacks: first, it is nonlinear, and second, it is implicit. Also, because of the mathematical nature, the measurands cannot be determined analytically but have to be estimated numerically. In the course of this process, evaluation errors, δU_i^{E}, occur caused by the systematic and random scatter of input data. Third, as can be shown experimentally, the ideal mathematical model, Eq. (1), is not valid for either short, $0 \leqslant t < t_{\min}$, or long, $t > t_{\max}$, times, because of the real strip's nonvanishing heat capacity and the real sample's exposed outer surfaces (cf. Section 2.1.1). As a first-order approximation, Eq. (1) is practically valid only for such a time interval during which the strip's thermal influence can be confined to the sample itself. Since this signal segment is not defined by theory, both its end points can be located by trial and error only. Hence, another two errors, namely, model and measurement errors, δU_i^{M} and δU_i^{J}, respectively, are introduced. The most significant errors of each of the three classes mentioned above are analyzed below. The overall deviation from an ideal THS signal, U_{i}*, is given by

$$U_i = U_i^* + \delta U_i = U_i^* + \delta U_i^{\mathrm{M}} + \delta U_i^{\mathrm{E}} + \delta U_i^{\mathrm{J}} \tag{5}$$

Here the superscripts denote the following potential sources of error: M, mathematical model; E, evaluation method; and J, measurement method.

2.1.1. Ideal-Model Errors

The THS experimental setup, as depicted in Fig. 1, cannot be treated analytically because it is subject to complex inner and outer boundary conditions. Therefore, the problem is replaced by the simpler one of a thermally closed system consisting of a perfect heat source embedded in a perfect heat sink. These assumptions ensure that the electric power, $P = UI$, fed to the two-dimensional strip, is completely and instantly liberated to

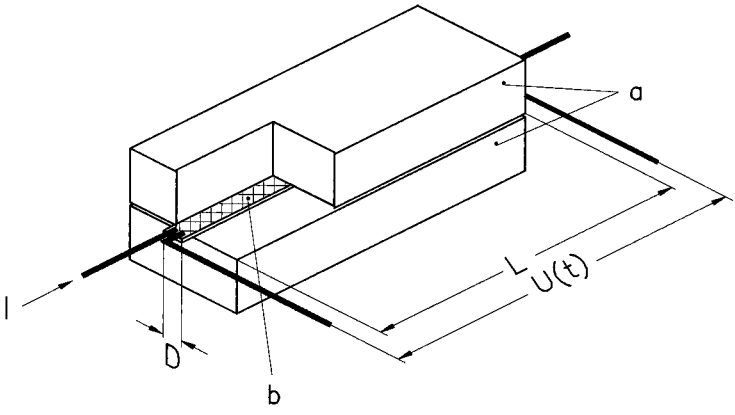

Fig. 1. Transient hot strip thermal part of setup. **a**, sample halves; **b**, hot-strip of width D and length L; I, electric current: $U(t)$, THS voltage signal.

the infinite sample as heat at a rate of $P = \Phi_0$. The complete heat is stored here, as given by $\int \Phi_P \, dt = \Delta Q$. The balance in the closed system is simply expressed by

$$\Phi_P = \Phi_0 \tag{6}$$

This major assumption finally leads to the mathematical model given below.

The actual THS setup may not be treated as a thermally closed system. The imperfections of both its components involve open inner and outer boundaries that can be crossed by stray heat flows Φ_{ii}: the three-dimensional strip acts not only as a source but also as an inner sink due to its nonvanishing heat capacity. The finite sample responds not only as a sink but also as an outer source because of its exposed surfaces. While the strip stores heat that flows "inward," namely, as Φ_{11}, the sample releases heat "outward," namely, heat at a net rate of $\Phi_{21} = (\Phi'_{21} - \Phi'_P)$. Here Φ'_P indicates the virtual heat flow inside an infinite sample that would flow instead of Φ'_{21} in a finite sample. Moreover, there is a third significant stray heat flow, Φ_{12}, that can leave the system through the heavy electrical leads. All of these heat flows depend on their characteristic temperature gradients and, hence, on time because of the transient nature of the experiment, $T = T(t)$. The balance of the open system is written

$$\Phi_p(T, t) = \Phi_0 - (\Phi_{11}(T, t) + \Phi_{12}(T, t) + \Phi_{21}(T, t) + \cdots) \tag{7}$$

As possible sources of error, the stray heat flows change the strip's temperature excursion and thus, the THS signal $\Delta U(t)$. As pointed out above, Φ_{11} becomes effective at short times and Φ_{21} at long times only: when the experiment is started, the inner stray heat flow, Φ_{11}, instantly increases enormously to heat up the strip, but within the next few seconds, it decreases to minor values (cf. Section 2.1.1.1). The outer stray heat flow, Φ_{21}, does not become significant before the heat flow Φ_P has traveled the sample completely and reaches its exposed surfaces. However, from that moment, Φ_{21} increases or decreases monotonically depending on the outer boundary conditions (cf. Sections 2.1.1.2). Thus, an "intermediate" time interval may be considered as the practically valid domain of Eq. (1). A substantial part of any nonlinear THS data analysis therefore concerns as precise a definition of this interval as possible.

In contrast to Φ_{11} and Φ_{21}, the heat flow Φ_{12} can be adjusted experimentally by using leads of appropriate diameter. When this is done, the temperature gradients at both ends of the strip can be minimized. Thus, Φ_{12} may be neglected. The deviations of the practical setup from the ideal model introduce two significant model errors:

$$\delta U_i^{\mathrm{M}} = \delta U_i^{\mathrm{W}}(\Phi_{11}) + \delta U_i^{\mathrm{R}}(\Phi_{21}) \tag{8}$$

Here the superscripts denote the following sources of error: W, open inner boundary; R, open outer boundary. There are other sources of model errors such as temperature-dependent sample properties, the strip's finite thickness and length, its finite thermal conductivity, the interfacial thermal resistance, etc. An analysis of these effects shows that they may be neglected compared with the above-mentioned major errors (cf., e.g., Ref. 6).

2.1.1.1. Inner Boundary (Three-Dimensional Strip). A metal strip of thickness v, volume $V = LDv$, density ρ^{S}, and specific heat capacity $c_{\mathrm{p}}^{\mathrm{S}}$ is able to store heat at a rate of $LDv\rho^{\mathrm{s}}c_{\mathrm{p}}^{\mathrm{s}}\ \mathrm{d}T^{\mathrm{s}}/\mathrm{d}t$. Supplied by a constant electrical power $P = \Phi_0$, there is therefore a stray heat flow Φ_{11} "into" the strip. Φ_{11} is stored and, thus, increases the strip's mean temperature T^{S}, which is a measure of its enthalpy H. The model error δU_i^{W} introduced by this phenomenon can be expressed in terms of the working equation [Eq. (1)],

$$\delta U_{i(\tau)}^{\mathrm{W}} = \frac{-\Phi_{11}(\tau)}{\Phi_0} kf(\tau_i) \tag{9}$$

where

$$\Phi_{11}(\tau) = \frac{\mathrm{d}H}{\mathrm{d}t} = LDv\rho^{\mathrm{s}}c_{\mathrm{p}}^{\mathrm{s}}\frac{\mathrm{d}T^{\mathrm{s}}}{\mathrm{d}t}$$

$$= \frac{v\rho^{\mathrm{s}}c_{\mathrm{p}}^{\mathrm{s}}\Phi_0}{\sqrt{\pi}\,\lambda}\sqrt{\frac{a}{t}}\left[\operatorname{erf}\left(\frac{1}{\tau}\right) + \frac{\tau}{\sqrt{\pi}}\exp\left(-\frac{1}{\tau^2}\right) - \frac{\tau}{\sqrt{\pi}}\right] \tag{10}$$

For very short times, within the limit $t \to 0$, Eq. (9) becomes $|\Phi_{11}/\Phi_0| \to 1$. Hence, at the moment the experiment is started, the input power is consumed totally by the strip. However, 1 s later the ratio of heat flows has decreased rapidly to typically $|\Phi_{11}/\Phi_0| \approx 1\,\%$ because of the strip's low heat capacity.

2.1.1.2. Outer Boundary (Finite Sample). In order to analyze the potential error introduced by the outer boundary of a finite sample, two cylindrical specimens of a homogeneous and isotropic dielectric (λ, a) are considered here. The first is unbounded. The second is of finite radius R_0 and perfectly embedded in an outer metallic sample holder. Both are considered for a THS experiment.

In the case of the finite sample, the heat, liberated by the strip, travels through the dielectric and, after some time, reaches the outer surface A. Here it leaves the thermal system under test for the sample holder as the stray heat flux $\Phi'_{21}(R_0, t)/A$. For the infinite sample, in complete accordance with the ideal model, the virtual cylinder surface A at radius R_0 is crossed by the flux $\Phi'_{\mathrm{P}}(R_0, t)/A$. Thus, the difference of both heat flows, $\Phi_{21}(t) = \Phi'_{21}(t) - \Phi'_{\mathrm{P}}(t)$, integrated with respect to time, provides an expression for the additional enthalpy stored by the sample. This enthalpy causes a deviation of the temperature of the real sample from that of the ideal one. Due to the transient nature of the experiment, $\Phi_{21}(t)$ depends nonlinearly on time.

In general, the above-mentioned thermal condition on the outer surface of a finite sample is neither adiabatic nor isothermal during a THS experiment. This is the case of a nonlinear boundary condition of the second kind:

$$\lambda_{\mathrm{M}}\left.\frac{\partial T}{\partial n}\right|_{R_0} = \frac{\Phi'_{21}(R_0, t)}{A} \tag{11}$$

where λ_{M} denotes the thermal conductivity of the sample holder and $\partial T/\partial n$ is the derivative along the outward drawn normal to the surface A. Here the heat flux Φ_{21}/A is not prescribed; it is searched. While $\Phi'_{\mathrm{P}}(R_0, t)/A$ can

be calculated from the ideal model, $\Phi'_{21}(t)$ can only be estimated. No solution for the practical case of a finite sample has so far been found. Nevertheless, taking into account that the thermal conductivity of the sample holder is much higher than that of the sample, $\lambda_M \gg \lambda$, the outer surface of the sample can be considered to be isothermal at the temperature $T = T_0$. Consequently, the difference from the temperature of the ideal sample is given by $\delta T = T_0 - T(R_0, t)$. Assuming that δT does not depend on position and applying the so-called thermometer equation $U = U_0(1 + \alpha T)$, the following is obtained:

$$\delta U_i^R(t) = \alpha U_0[T_0 - T(R_0, t)] \tag{12}$$

If the sample radius is large compared with the strip's half-width, $R_0 \gg D/2$, Eq. (1) reduces to the known solution for a linear heat source (cf., e.g., Ref. 5). From this, the following governing equations result for $T(R_0, t)$:

$$\delta U_i^R(t) = \alpha U_0 \frac{U_0 I}{4\pi\lambda L} \operatorname{Ei}\left(\frac{-R_0^2}{4at}\right) \tag{13}$$

$$\frac{\delta U_i^R(t)}{U} \approx \frac{\delta U_i^R(t)}{U_0} = \alpha \frac{\Phi}{4\pi\lambda L} \operatorname{Ei}\left(-\frac{R_0^2}{4at}\right) \tag{14}$$

Empirically, it can be shown that the exponential integral $-\operatorname{Ei}(-R_0^2/4at)$ does not have an effect on the error δU_i^R for arguments $R_0^2/4at < 0.5$. This is the case for a maximum excess temperature of the surface A of about 0.1 K. From $R_0^2/4at \approx 0.5$, the error begins to increase rapidly with time. An experiment should, therefore, be terminated at $t_{max} \leqslant R_0^2/2a$. This time is in good agreement with the Gustafsson proviso [7]: as a condition to terminate the experiment, Gustafsson empirically defines a probing depth $\Delta \approx \beta\sqrt{at_{max}}$, where $\Delta \approx R_0$. The value of the coefficient β is somewhat arbitrary between $\beta = 1.42$ and $\beta = 3$. t_{max} denotes the maximum duration of an experiment. However, the outer boundary error δU_i^R cannot be derived from this equation.

In general, the value of the thermal diffusivity a is not known and the time t_{max} for an experiment to be terminated cannot, therefore, be calculated. It must rather be estimated by trial and error.

2.1.2. Nonlinear Evaluation Errors

The nonlinear evaluation procedure to be applied for finding the numerical values of the measurands λ and a from any THS signal is described in detail elsewhere [3]. The criterion used there is to estimate the true values of the components of vector $\vec{b} = (U_0, k, a, t_0)$ so as to minimize

the sums of squares of deviations of the pointwise observed values $U_i = U(t_i)$ from these estimates $U(t_i, \vec{b})$:

$$\chi^2(\vec{b}) = \sum [\, U_i - U_0 - kf(\tau(t_i))\,]^2 = \sum [\, U_i - U(t_i, \vec{b})\,]^2 \to \text{Min} \tag{15}$$

A reliable numerical solution to Eq. (15) is obtained by using the Levenberg–Marquardt algorithm [3]. The regression model is given by the working equation, Eq. (1); the input data pairs are taken only from the valid time interval of a monitored signal. However, since these values are subject to random and systematic errors, the sets $U(t_i)$ and U_i always deviate. These errors can be analyzed in terms of the efficiency of the estimation, the variance $\chi^2(\vec{b})$. A measure of the precision of the fitted parameters, $\vec{b}$, is then given by the confidence interval $\vec{b} \pm u_A(\vec{b})$ that has to be related to the percentage confidence level 100 P [8]. This interval defines the region which includes the true parameter values with the probability P. The confidence interval associated with each single parameter b_m is calculated from the value of the standard deviation χ and the related element α^*_{mm} of the inverted Hessian $[\alpha^*] = [\alpha]^{-1}$:

$$u_A^2(b_m) = F(P, j)\,\frac{\chi^2}{N-j}\,\alpha^*_{mm} \tag{16}$$

Here $F(P, j)$ is a function of probability P and the degree of freedom j. For a confidence level of 68.3 %[3] and $j = 4$, $F(0.683,4) = 4.72$ is obtained. At this level, the relative errors in both measurands are given by

$$\frac{u_A(\lambda)}{\lambda} = \sqrt{\frac{4.72\chi^2}{k^2(N-4)}}\,\sqrt{\alpha^*_{22}} \tag{17}$$

$$\frac{u_A(a)}{a} = \sqrt{\frac{4.72\chi^2}{k^2(N-4)}}\,\frac{k}{a}\,\sqrt{\alpha^*_{33}} \tag{18}$$

In the case of a perfect data set, $\chi = 0$ is valid and the error in both measurands, therefore, vanishes. A perfect data set agrees unconditionally with the mathematical model and is not affected by any measurement error. For a data set that is affected by measurement errors, characterized by random deviations of U_i from the perfect data set, the ratio $\chi/(N-4) \approx \chi/N$ remains constant. Thus, the errors in the measurands λ and a can be

[3] A 68.3 % confidence interval is chosen for now. In Section 5, the evaluation error is added to all the other errors discussed here and the sum is then multiplied by a coverage factor of 2. This leads to a common confidence level of 95 %.

analyzed for any given time interval $[0, \tau_{\max}]$ in terms of the nondimensional expressions $\sqrt{\alpha^*_{22}}$ and $k/a\sqrt{\alpha^*_{33}}$, respectively. For this purpose, first, a constant and equally spaced sampling interval $\Delta t = t_{i+1} - t_i$ for the data acquisition is assumed. Two cases must then be considered, an infinite and a finite sample: for the finite sample, the maximum duration of an experiment has to be limited to $t_{\max} = N\,\Delta t$. Nevertheless, at any given value of N, e.g., $N = 1000$, $\tau_{\max}$ can be varied by choosing an appropriate value for the strip width D [cf. Eq. (4)]. In the case of the infinite sample, the duration is unlimited. Hence, any value for $\tau_{\max}$ can be prescribed for a constant strip width by varying $t_{\max}$. Since $N \propto \tau^2_{\max}$, $N = 500\tau^2$ is assumed, for example.

The solutions obtained for both above-mentioned cases, are graphically represented in Fig. 2. The nondimensional errors $\sqrt{\alpha^*_{22}}$ and $k/a\sqrt{\alpha^*_{33}}$ appear in terms of the upper end point of the time interval $[0, \tau_{\max}]$. On the basis of the curves, the following practical proviso can be made: if only the thermal conductivity of a material is of interest, the strip should be as narrow as possible; if the thermal diffusivity is needed as well, the strip width should be optimized according to the minimum of curve f_1.

The estimation errors are further discussed in Section 4.1 since they have to be estimated numerically along with the measurands.

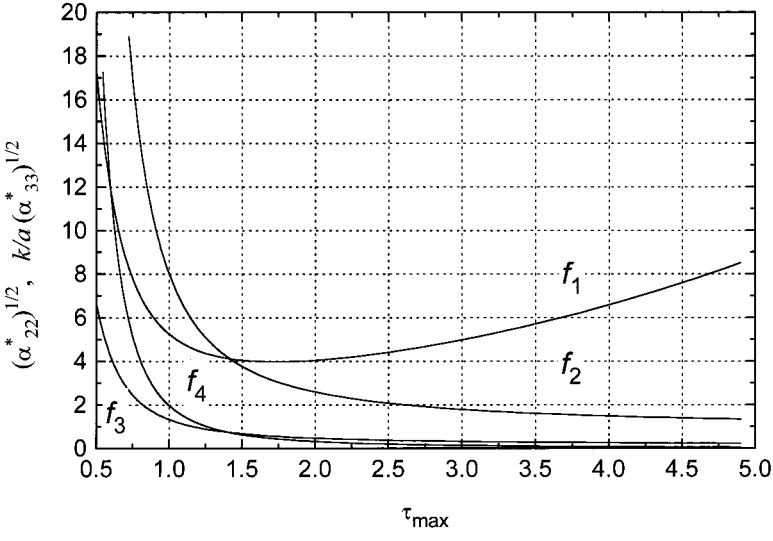

Fig. 2. Nondimensional coefficients $(\alpha^*_{22})^{1/2}$ (λ: curves f_3 and f_4) and $k/a(\alpha^*_{33})^{1/2}$ (a: curves f_1 and f_2) vs the upper end point $\tau_{\max}$ of nondimensional time interval $[0, \tau_{\max}]$. f_1 and f_3, $N = 1000$; f_2 and f_4, $N = 500\tau^2_{\max}$ (see text).

2.2. Linearized Model

Due to the nonlinear and implicit mathematical character of Eq. (1), the complex numerical estimation procedure mentioned above is required for a THS data analysis. Furthermore, since in practice the classical model (Eq. (1)) breaks down for both short and long times t, the nonlinearly time-dependent model errors, $\delta U_i^{\mathrm{W}}(t)$ and $\delta U_i^{\mathrm{R}}(t)$, are introduced. They can be estimated only roughly. In order to circumvent both of these severe problems, a quasi-linear approximation function F has been derived which replaces the shape function $f(\tau)$ [4].

Linearization of Eq. (1) starts by expressing the functions f_1 and f_2 of Eq. (2) by a first-order Taylor series, while function f_3 is expanded in a McLaurin series. As discussed below, for values of $1/\tau$ which are small compared with unity, it is sufficient to retain only the first two terms of each series f_1 and f_2 and the first three terms of f_3 for linearization and subsequent evaluation of the related model error.

$$f_1: \qquad \tau \operatorname{erf}\left(\frac{1}{\tau}\right) \approx \frac{2}{\sqrt{\pi}} - \frac{2}{\sqrt{\pi}} \frac{1}{3\tau^2} \tag{19}$$

$$f_2: \qquad -\frac{\tau^2}{\sqrt{4\pi}}\left[1 - \exp\left(-\frac{1}{\tau^2}\right)\right] \approx -\frac{1}{2\sqrt{\pi}} + \frac{1}{4\sqrt{\pi}\cdot\tau^2} \tag{20}$$

$$f_3: \qquad -\frac{1}{\sqrt{4\pi}} \operatorname{Ei}\left(-\frac{1}{\tau^2}\right) \approx \frac{1}{\sqrt{4\pi}}\left[-\gamma + 2\ln\tau + \frac{1}{\tau^2}\right] \tag{21}$$

Here $\gamma = 0.5772\ldots$ is Euler's constant. The first term of each f_1 and f_2 series expansion is identical to the limiting value of these two rapidly converging series. After summing, the approximation

$$f(\tau) \approx \frac{3-\gamma}{2\sqrt{\pi}} + \frac{1}{\sqrt{\pi}} \ln\tau + \frac{1}{12\sqrt{\pi}\,\tau^2} \tag{22}$$

is included in Eq. (1). The voltage signal is then given by

$$U(t) - U_0 \approx \frac{\alpha U_0^2 I}{4\pi L\lambda}\left(3 - \gamma + \ln t + \ln\frac{4a}{D^2} + \frac{D^2}{24at}\right) = m\ln t + n + R_2(t) \tag{23}$$

where $m = \alpha U_0^2 I/4\pi L\lambda$, $n = m(3 - \gamma + \ln 4a/D^2)$, and $R_2 = mD^2/24at$. This expression can be linearized, first, by transforming $\ln t \to t'$ and, second, by

neglecting the third term on the right-hand side, $R_2(t)$, because it rapidly vanishes as the nondimensional time τ increases:

$$\frac{R_2(t)}{m \ln t + n} = \frac{1}{(3 - \gamma + \ln \tau^2)\, 6\tau^2} \tag{24}$$

As a measure of the first-order deviation of the linear approximation from its origin, R_2 is analyzed below. Finally, the quasi-linear working equation, given in terms of real time t, reads

$$U(t) - U_0 \approx \frac{\alpha U_0^2 I}{4\pi L \lambda} \left(\ln t + \ln \frac{45a}{D^2} \right) = mt' + n \tag{25}$$

Here m and n are the line segment's slope and intercept, respectively. From any THS signal, $\Delta U_i(t)$, both parameters can be determined according to

$$m = \frac{\sum t_i' \sum \Delta U_i - N \sum t_i' \, \Delta U_i}{(\sum t_i')^2 - N \sum t_i'^2} \tag{26}$$

and

$$n = \frac{1}{N} \left(\sum \Delta U_i - m \sum t_i' \right) \tag{27}$$

respectively. The measurands follow from

$$\lambda = \frac{\alpha U_0^2 I}{4\pi L m} \tag{28}$$

and

$$a = \frac{D^2}{45} \exp\left(\frac{n}{m} \right) \tag{29}$$

Here, $\Delta U_i = U_i - U_0$ and $t_i' = \ln t_i$, while N indicates the magnitude of the data set to be analyzed.

Figure 3 shows two functions for different stages of the approximation of $f(\tau)$, namely, F_1 and F_2. F_1 is obtained by summarizing the first series terms on the right-hand side of f_1 and f_2 [Eqs. (19) and (20)] along with f_3, as given on the left-hand side of Eq. (21) in its original form:

$$F_1(t) := \frac{1}{2\sqrt{\pi}} [3 - \mathrm{Ei}(-\tau^{-2})] \tag{30}$$

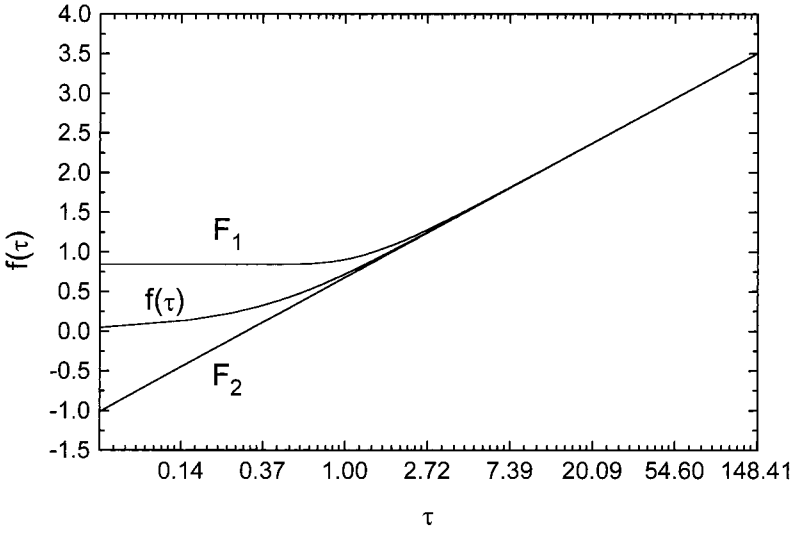

Fig. 3. Shape function $f(\tau)$ and substitutes F_1 and F_2, plotted vs $\ln \tau$ (see text).

The final result is written as follows:

$$F_2(t) := \frac{1}{2\sqrt{\pi}}\left(3 - \gamma + \ln t + \ln\frac{4a}{D^2}\right) = \frac{1}{2\sqrt{\pi}}\left(\ln\frac{45at}{D^2}\right) \tag{31}$$

As can be seen from Fig. 4, which shows the relative error $[F_2(\tau) - f(\tau)]/f(\tau)$ vs τ, the approximation function, F_2, is valid for nondimensional times $\tau > 2$. Therefore, the practical proviso is made that all data pairs $U_i(\tau)$ of a THS signal for which $\tau \leqslant 2$ are discarded from all subsequent analyses.

Due to the linear approximation, another model error, δU_i^{L}, is introduced that has to be taken into account subsequently. However, as shown later, despite this additional term, the overall uncertainty of the linear method is almost the same as that of the nonlinear method because the linearization introduces only a small additional error. In general, the linear method uncertainty can even be smaller because the above-mentioned model errors, $\delta U_i^{\mathrm{R}}(\tau)$ and $\delta U_i^{\mathrm{W}}(\tau)$, do not have to be taken into account: the error $\delta U_i^{\mathrm{R}}(\tau)$, which is connected with the inner boundary, does not become effective for times $\tau > 1$. The error $\delta U_i^{\mathrm{W}}(\tau)$, being connected with the outer boundary, gives rise to nonlinear deviations at large times. These can now be easily detected as a departure from linearity of the plot U_i vs. $\ln t$ (cf. Fig. 9).

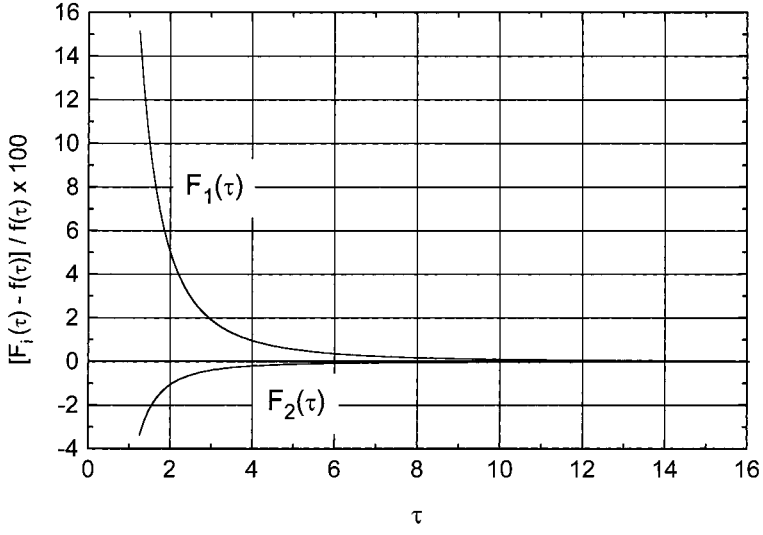

Fig. 4. Deviation of F_1 and quasi-linear function F_2 from the THS shape function $f(\tau)$ (see text).

2.2.1. Linearized Model Error

In the course of the mathematical treatment of $f(\tau)$ that leads via F_1 to F_2, an error is introduced into Eq. (25), namely, the linearized model error. In Fig. 4, the individual truncation errors of $F_1(\tau)$ and $F_2(\tau)$ are plotted as the percentage deviation from their common origin $f(\tau)$. Surprisingly, the absolute departure of the logarithmic (ln-) function F_2 is smaller than that of the exponential integral (Ei-) function F_1. This unexpected behavior is due to the truncation error of the McLaurin series of f_3 that is opposite in sign and, therefore, has a compensating effect [cf. Eq. (21)]. The absolute ratio of both truncation errors is given by

$$\left|\frac{F_1(\tau)-f(\tau)}{F_2(\tau)-f(\tau)}\right| \approx 5 \tag{32}$$

The approximation of F_1 [cf. Eq. (30)] that leads to the final solution F_2 [cf. Eq. (31)] obeys the same rules as the linearization to the fundamental transient hot wire (THW) model, $f_{\mathrm{W}}(\tau)$. From Ref. 5, for example, it is known that

$$f_{\mathrm{W}}(\tau) = -\mathrm{Ei}(-\tau_{\mathrm{r}}^{-2}) \approx -\gamma + 2\ln\tau_{\mathrm{r}} = -\gamma + \ln\frac{4at}{r^2} =: F_{\mathrm{W}} \tag{33}$$

Here r denotes the radius of the wire (instead of D, the width of the strip). The ratio of the absolute approximation errors related to both methods, THS and THW, reads as follows:

$$\frac{F_W(\tau) - f_W(\tau)}{F_2(\tau) - f(\tau)} = Q(\tau) \approx 21 \tag{34}$$

or $Q(\tau) \approx 3$ if the radius of the wire r is related to the half-width $D/2$ of the strip. Thus, the linearization of the THS working equation yields an even better approximation than that of the closely related THW method. Figure 5 shows the percentage departure of F_W from f_W vs nondimensional time.

From the data set, $(F_2(\tau) - f(\tau))/f(\tau)$, as plotted in Fig. 4, the individual linear model error cannot be derived directly because it depends not only on $\tau_{min}(t_{min})$, but also on the other end point, $\tau_{max}(t_{max})$, of a signal's linear segment $[\tau_{min}, \tau_{max}]$ (cf. Fig. 11). Since this error is introduced by the truncation of the series of f_1, f_2, and f_3, it can be expressed to a good approximation by the above-mentioned remainder R_2. Expressed in terms of the time-dependent error in voltage $\delta U_i^L(t)$, one obtains for each individual experimental data pair $U_i(t)$:

$$\delta U_i^L(t_i) = \frac{D^2 m}{24 a t_i} = \frac{m}{6 \exp(n/m - 3 + \gamma) \exp t_i'} \tag{35}$$

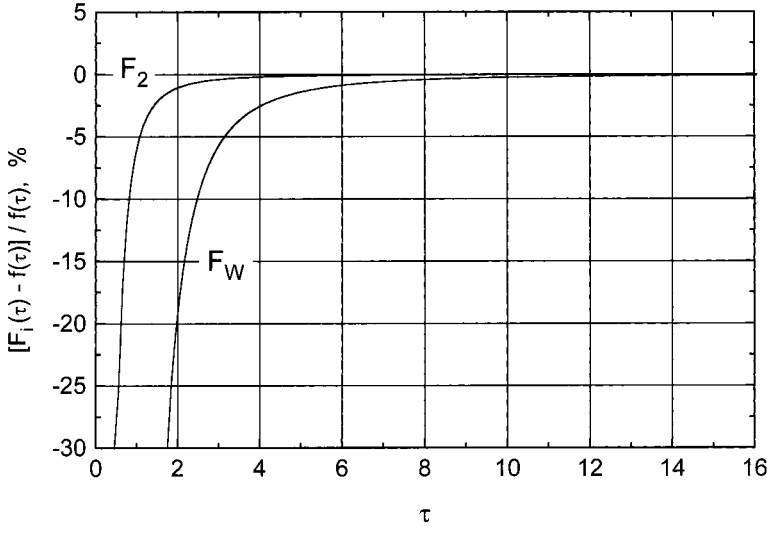

Fig. 5. Deviation of quasi-linear function F_W from the THW shape function $f_W(\tau)$ compared with the THS shape function F_2 (see above).

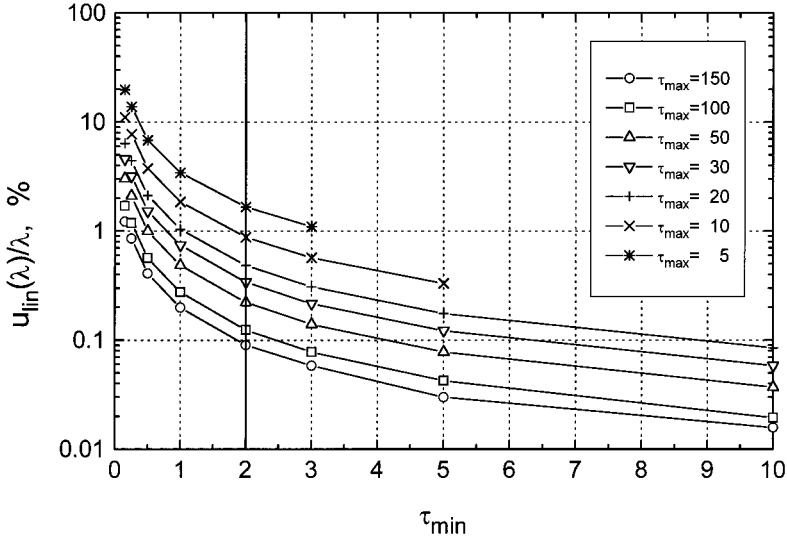

Fig. 6. Model error in measured thermal conductivity λ caused by the linearization of Eq. (1). The error has been plotted in terms of different upper end points τ_{max} of any linear interval.

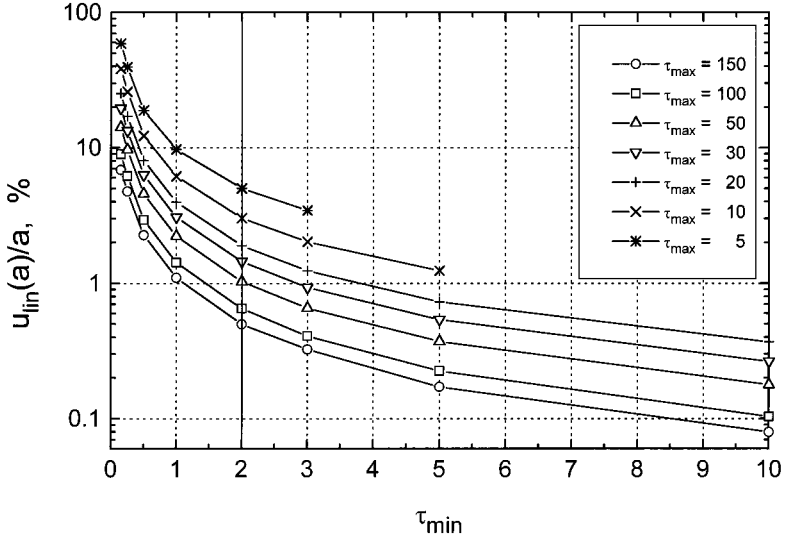

Fig. 7. Model error in measured thermal diffusivity a caused by the linearization of Eq. (1). The error has been plotted in terms of different upper end points τ_{max} of any linear interval.

For the linear segment of a THS signal to be analyzed, the induced deviations from both measured quantities, m and n, are given by

$$u_{\mathrm{lin}}(m) = \frac{m}{6\exp(n/m - 3 + \gamma)} \frac{\sum t_i' \sum \exp(-t_i') - N \sum t_i' \exp(-t_i')}{(\sum t_i')^2 - N \sum t_i'^2} \tag{36}$$

$$u_{\mathrm{lin}}(n) = \frac{1}{N}\left[\frac{m}{6\exp(n/m - 3 + \gamma)} \sum \exp(-t_i') - m \sum t_i' \right] \tag{37}$$

A numerical evaluation of Eqs. (36) and (37) with respect to the measurands λ and a results in the following empirical expressions:

$$u_{\mathrm{lin}}\frac{(\lambda)}{\lambda} 100 \approx L1(\tau_{\min} \tau_{\max}^{L2})^{-1} \tag{38}$$

$$\frac{u_{\mathrm{lin}}(a)}{a} 100 \approx A1(\tau_{\min} \tau_{\max}^{A2})^{-1} \tag{39}$$

Here the constants are $L1 = 12.7$, $L2 = 0.85$, $A1 = 28.5$, and $A2 = 0.67$. Separately for both measurands, Figs. 6 and 7 show the effect which a variation of the upper end point $\tau_{\max}$ between 5 and 150 exerts on the

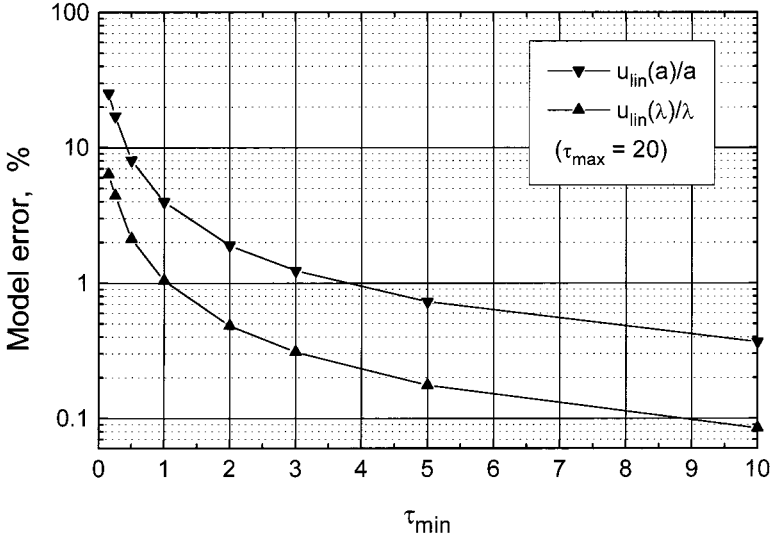

Fig. 8. Percentage model error in measured thermal conductivity λ and thermal diffusivity a caused by the linearization of Eq. (1) for an upper end point $\tau_{\max} = 20$. The error has been plotted vs the lower end point of any linear time interval (see text).

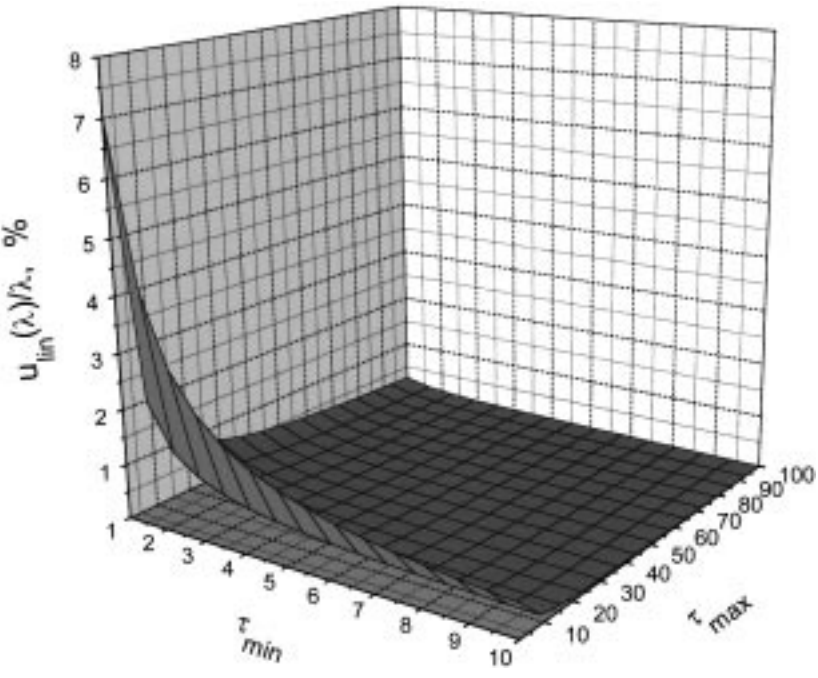

Fig. 9. Model error in measured thermal conductivity caused by the linearization of Eq. (1). The error has been plotted vs the end points τ_{min} and τ_{max} of any linear interval.

related model error in terms of the lower end point τ_{min}. For a more convenient comparison, numerical values of $\delta\lambda/\lambda$ and $\delta a/a$ vs. τ_{min} are plotted in Fig. 8 for a fixed value of $\tau_{max} = 20$. Obviously, the model error connected with thermal diffusivity is larger than that connected with thermal conductivity. This has been pointed out more generally in Ref. 3 for the first time.

As mentioned above, the lower limit τ_{min} is proposed to equate to, at least, 2. The upper limit τ_{max} depends on the probing depth R_0 of the strip's thermal influence (i.e., the maximum sample width) and the strip width D, as discussed in Section 1. There, the empirically obtained Gustafsson expression [2]

$$\tau_{max} \approx \sqrt{2}\,\frac{R_0}{D} \tag{40}$$

is given along with our linear approximation of the related maximum excess temperature, $T_A \approx 0.1\ K$, of the sample's exposed surface A at the

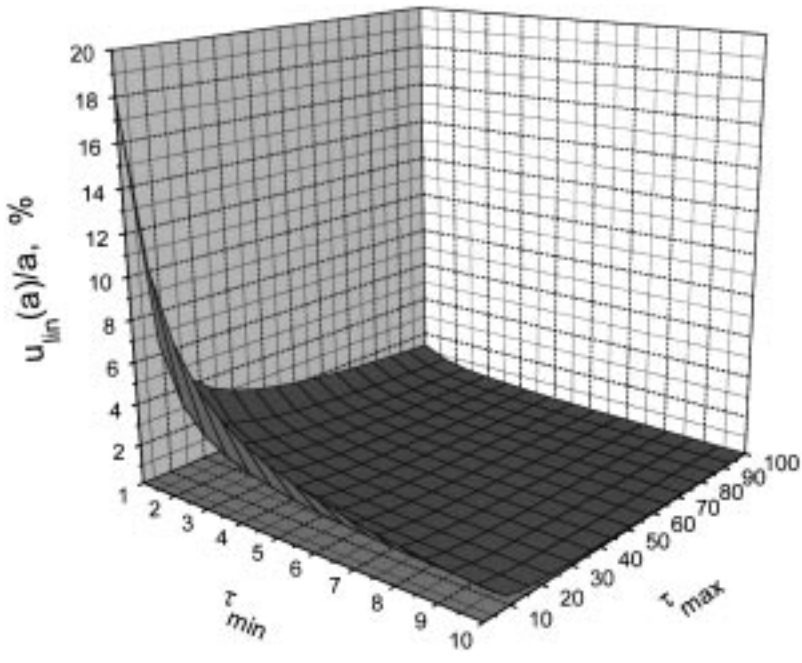

Fig. 10. Model error in measured thermal diffusivity caused by the linearization of Eq. (1). The error has been plotted vs the end points $\tau_{\min}$ and $\tau_{\max}$ of any linear interval.

nondimensional time $\tau_{\max}(t_{\max})$. This value is in excellent agreement with the experiment, as shown in Fig. 11.

2.2.2. Linear Evaluation Error

As has been shown for the nonlinear model parameters $k(\lambda)$ and a, the linearized model parameters m and n can also be estimated only with a restricted degree of confidence, expressed here in terms of the confidence intervals $u_A(m)$ and $u_A(n)$, respectively, given by Eq. (16). These intervals are again associated with the characteristic confidence level P.

In the case of linear regression ($j=2$) and, again, a percentage confidence level of $P=68.3\%$, the probability function now results in $F(0.683,2)=2.3$ [8], and both diagonal elements of the matrix α^* are

$$\alpha_{11}^* = \frac{\sum t_i'^2}{N\sum t_i'^2 - (\sum t_i')^2} \tag{41}$$

$$\alpha_{22}^* = \frac{N}{N\sum t_i'^2 - (\sum t_i')^2} \tag{42}$$

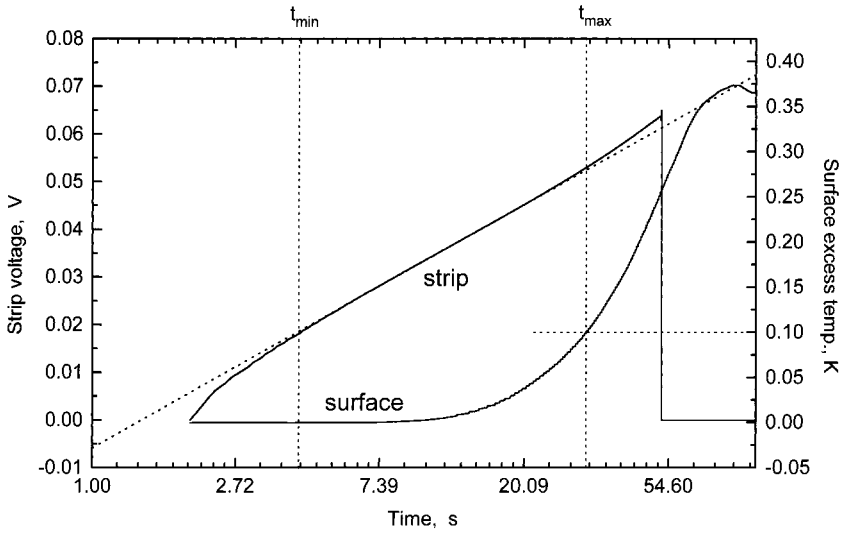

Fig. 11. Experimental THS signal (strip voltage) and excess temperature of the sample's outer surface, both plotted vs ln t (see text).

Substituting Eq. (41) and Eq. (42), respectively, into Eq. (16), the confidence intervals for slope m and intercept n, referred to as standard uncertainties of type A, are written as follows:

$$u_{\mathrm{A}}(m) = \sqrt{\frac{2.3\chi^2}{N-2}\frac{N}{N\sum t_i'^2 - (\sum t_i')^2}} \tag{43}$$

$$u_{\mathrm{A}}(n) = \sqrt{\frac{2.3\chi^2}{N-2}\frac{\sum t_i'^2}{N\sum t_i'^2 - (\sum t_i')^2}} \tag{44}$$

3. MEASUREMENT ERRORS

There are four significant measurement errors that have to be taken into account. Three of them originate in the electrical part of the setup. First, to simplify the experiment, the strip is not heated by constant power but by constant current. This mode results in a continuous growth of the strip's heat flow Φ_0, which is given by $\Phi_0 = P = R(T)I^2$. Second, the current source's instability, δI, causes a departure of the THS voltage signal, namely, $U_i\,\delta I/I$. This error is analyzed together with the voltage measurement error (cf. Section 3.2): due to the limited accuracy and non-vanishing integration time of the voltmeter, the measurement is affected by an error δU_i^{V}. Third, an additional error in the measured voltage arises

from a temperature drift in the sample that occurs even in well-thermostated setups:

$$\delta U_i^{\mathrm{J}} = \delta U_i^{\mathrm{P}} + \delta U_i^{\mathrm{V}} + \delta U_i^{\mathrm{T}} \tag{45}$$

Here the superscripts denote the following potential sources of error: P, constant current mode; V, nonideal voltmeter, instability of current source; and T, temperature drift.

3.1. Constant-Current Mode

The electrical resistance $R(T)$ of the Joule-heated strip increases continuously as a measure of its temperature T. When a constant current I is fed to the strip, it generates a heat flow that is not constant but varies at a rate $\Phi_0 = P = UI = R(T)I^2$. This effect causes an error δU_i^{P} in the measured voltage signal.

To determine the influence of the temperature-dependent generation rate within Eq. (1), the constant power $U_0 I$ is replaced by $U(t)I_0$. After some rearrangements the working equation reads as follows:

$$U(t) = \frac{U_0}{1 - (k/U_0)\, f(\tau)} \tag{46}$$

A Taylor series expansion of $U(t)$ about $kf(\tau)/U_0$ can be used to determine the error since $kf(\tau)/U_0 \ll 1$:

$$U(t) = U_0 + kf(\tau) + \frac{k^2}{U_0} f^2(\tau) + \cdots \tag{47}$$

The difference between Eq. (1) and Eq. (47) is represented by the third term on the right-hand side of Eq. (47) because higher-order terms may be neglected in view of the above-mentioned inequality. Thus,

$$\delta U_i^{\mathrm{P}} = \frac{k^2}{U_0} f^2(\tau) \tag{48}$$

In terms of the nondimensional time τ, three cases can be considered:

1. $$\tau \ll 1 \Rightarrow \delta U_i^{\mathrm{P}} = \frac{k^2}{U_0} \tau^2 \tag{49}$$

$$2. \qquad \tau = 1 \Rightarrow \delta U_i^{\mathrm{P}} = 0.53 \frac{k^2}{U_0} \tag{50}$$

$$3. \qquad \tau \gg 1 \Rightarrow \delta U_i^{\mathrm{P}} = \frac{k^2}{\pi U_0} (1.21 + \ln \tau)^2 \tag{51}$$

During a normal THS run, all three cases occur, one after the other.

3.2. Voltage Measurement

Errors in the measured voltage, δU_i^{V}, of the monitored signal $U(t_i)$ are caused mostly by three different effects: the finite precision of the voltmeter, $u(U)$; its nonvanishing integration time δt while the signal rises as $k(\partial f(\tau_i)/\partial t)$; and the current source uncertainty, $u(I)$. Both instrument uncertainties, $u(U)$ and $u(I)$, depend on time. Their systematic components are covered by Eq. (1). Their random components cause an increase in the χ^2 deviations of the observed signal from the fitted one. As A-type uncertainties, they have already been accounted for in Section 2.1.2. Thus, the residual time-dependent voltage error is introduced by the integration time of the voltmeter and the transient signal rise:

$$\delta U_i^{\mathrm{V}} = \delta t \, k \frac{\partial f(\tau_i)}{\partial t} \tag{52}$$

where

$$\frac{\partial f(\tau_i)}{\partial t} = \frac{\partial f(\tau)}{\partial \tau} \frac{\partial \tau}{\partial t}\bigg|_{t=t_i} = \frac{\tau_i}{2t_i} \left[\operatorname{erf} \frac{1}{\tau_i} + \frac{\tau_i}{\sqrt{\pi}} \exp\left(-\frac{1}{\tau_i^2} \right) - \frac{\tau_i}{\sqrt{\pi}} \right] \tag{53}$$

During a THS run, the first term on the right-hand side of Eq. (52) increases slightly, the second term remains constant, and the third term decreases to 50% of its initial value within the interval $(0, \tau = 1)$.

.

3.3. Ambient Temperature Variation

Any variation in the temperature of the sample environment, $\mathrm{d}T_{\mathrm{D}}/\mathrm{d}t$, causes a departure in the measured voltage signal of

$$\delta U_i^{\mathrm{T}} = \alpha U_0 \frac{\mathrm{d}T_{\mathrm{D}}}{\mathrm{d}t} t_i \tag{54}$$

4. STANDARD UNCERTAINTY

According to Ref. 1, the combined standard uncertainty $u_c(y)$ of the quantity y is the positive square root of the combined variance $u_c^2(y)$ obtained from

$$u_c^2(y) = \sum_{i=1}^{N} \left(\frac{\partial F}{\partial x_i} \right)^2 u^2(x_i) \tag{55}$$

Here $F(x_i)$ denotes the (explicit) model of the measuring procedure of input quantities x_i. The partial derivatives of F with respect to x_i are referred to as sensitivity coefficients.

For the classical THS working equation [Eq. (1)] as the function F, the right-hand side of Eq. (55) cannot be treated analytically because of its implicit character in both measurands. Therefore, a numerical procedure has been developed to estimate the variances $u^2(x_i)$ as close as possible to the recommendations of the ISO guide. This procedure is presented in the following section. In contrast to Eq. (1), its explicit approximation, Eq. (25), can be analyzed in full accordance to the guide, as presented in Section 4.2.

4.1. Standard Uncertainty of the Nonlinear Method

In cases of an implicit model, the ISO guide [1] recommends that the particular values of the derivatives (sensitivity coefficients) of Eq. (55) be evaluated experimentally. However, in the case of THS measurements, this procedure is a tedious and time-consuming task that easily results in inaccurate results. The experimental approach is therefore transformed into a numerical procedure. Within the framework of the nonlinear data analysis mentioned above, the specific response of the estimator is calculated for systematic variations of any single input quantity, while, for each run, all other quantities remain unaltered. Since the resulting characteristic variances would not describe deviations due to the numerical procedure itself, they have to be separated into a type A subcomponent, u_A^2, and a type B subcomponent, u_B^2, prior to the computation. The type A values stand for the evaluation errors, while the type B values provide a measure of the possible errors of model and measurement.

The primary input quantity is given by the pointwise monitored THS signal (U_i, t_i), assuming that model, Eq. (1), is valid for the measuring procedure. For the measurands it then follows that

$$\lambda = \frac{\alpha U_0^2 I}{2\sqrt{\pi}\, Lk} \qquad \text{and} \qquad a = \frac{(\tau D)^2}{4t}$$

Hence, additional measurable quantities are α, U_0, I, L, D, and k. The combined variance in λ is given by

$$\left(\frac{u(\lambda)}{\lambda}\right)^2 = \left(\frac{u(\alpha)}{\alpha}\right)^2 + \left(\frac{u(I)}{I}\right)^2 + \left(\frac{u(L)}{L}\right)^2 + \left(2\,\frac{u(U_0)}{U_0}\right)^2 + \left(\frac{u(k)}{k}\right)^2 \tag{56}$$

The first four terms on the right-hand side of Eq. (56) can be readily evaluated. The last one, $u(k)$, requires separation into subcomponents which must be calculated individually. The same applies to the variance of a, Eq. (58).

$$\left(\frac{u(k)}{k}\right)^2 = \left(\frac{u_{\mathrm{A}}(k)}{k}\right)^2 + \left(\frac{u_{\mathrm{B}}(k)}{k}\right)^2 \tag{57}$$

$$\left(\frac{u(a)}{a}\right)^2 = \left(\frac{u_{\mathrm{A}}(a)}{a}\right)^2 + \left(\frac{u_{\mathrm{B}}(a)}{a}\right)^2 \tag{58}$$

The two type A variances are calculated from Eqs. (17) and (18), respectively:

$$u_{\mathrm{A}}^2(k) = 4.72\ |\alpha_{22}^*|\ \frac{\chi^2}{N-4} \tag{59}$$

$$u_{\mathrm{A}}^2(a) = 4.72\ |\alpha_{33}^*|\ \frac{\chi^2}{N-4} \tag{60}$$

The two type B variances are given by

$$u_{\mathrm{B}}^2(k) = u_{\mathrm{w}}^2(k) + u_{\mathrm{R}}^2(k) + u_{\mathrm{P}}^2(k) + u_{\mathrm{v}}^2(k) + u_{\mathrm{T}}^2(k) \tag{61}$$

$$u_{\mathrm{B}}^2(a) = \left(2\,\frac{a}{D}\,u(D)\right)^2 + u_{\mathrm{w}}^2(a) + u_{\mathrm{R}}^2(a) + u_{\mathrm{P}}^2(a) + u_{\mathrm{v}}^2(a) + u_{\mathrm{T}}^2(a) \tag{62}$$

The subscripts denote the following possible sources of error: W, inner boundary; R, outer boundary; P, constant-current mode; V, nonideal voltmeter/current source; and T, temperature drift.

To perform the above-mentioned numerical operation on Eqs. (61) and (62), both expressions are taken as operands. Two operators, G and H, are introduced that define a mapping between a THS time series $(\Delta U_i, t_i)$ and the estimates of the related parameters $k(\lambda)$ and a:

$$k = G(U_i, t_i) \tag{63}$$

$$a = H(U_i, t_i) \tag{64}$$

These numerical operators are given by the above-mentioned Levenberg–Marquardt estimator.

The estimator's initial run yields the measurands k and a from the original THS signal U_i to be analyzed. Prior to a second run, the signal is altered by pointwise adding the individual value of one particular error, e.g., δU_i^{W}. The estimator's new output then results in

$$k_1 = G(U_i + \delta U_i^{\mathrm{W}}, t_i) \qquad \text{and} \qquad a_1 = H(U_i + \delta U_i^{\mathrm{W}}, t_i) \tag{65}$$

It follows that

$$\begin{aligned} u_{\mathrm{W}}(k) &= |G(U_i, t_i) - G(U_i + \delta U_i^{\mathrm{W}}, t_i)| \\ u_{\mathrm{W}}(a) &= |H(U_i, t_i) - H(U_i + \delta U_i^{\mathrm{W}}, t_i)| \end{aligned} \tag{66}$$

Subsequent runs provide all required variances.

4.2. Standard Uncertainty of the Linear Method

For the linear method all sensitivity coefficients can readily be calculated analytically. From Eq. (25), working equations are readily derived for both measurands [Eqs. (28) and (29)]. The combined variances for λ and a are obtained from the time-independent standard uncertainties of the input quantities and the linearized model errors:

$$\left(\frac{u_{\mathrm{c}}(\lambda)}{\lambda}\right)^2 = \left(\frac{u(\alpha)}{\alpha}\right)^2 + \left(\frac{u(I)}{I}\right)^2 + \left(\frac{u(L)}{L}\right)^2 + \left(\frac{u(U_0)}{U_0}\right)^2 + \left(\frac{u(m)}{m}\right)^2 + \left(\frac{\delta\lambda}{\lambda}\right)^2 \tag{67}$$

$$\left(\frac{u_{\mathrm{c}}(a)}{a}\right)^2 = \left(2\,\frac{u(D)}{D}\right)^2 + \left(\frac{n}{m}\,\frac{u(n)}{n}\right)^2 + \left(\frac{n}{m}\,\frac{u(m)}{m}\right)^2 + \left(\frac{\delta a}{a}\right)^2 \tag{68}$$

The model errors are taken into account in each case by the last term on the right-hand sides of both equations. The variances of input quantities α, I, L, U_0, and D can readily be calculated, whereas those of the parameters m and n consist of two subcomponents of type A and type B according to [1]

$$\left(\frac{u(m)}{m}\right)^2 = \left(\frac{u_{\mathrm{A}}(m)}{m}\right)^2 + \left(\frac{u_{\mathrm{B}}(m)}{m}\right)^2 \tag{69}$$

$$\left(\frac{u(n)}{n}\right)^2 = \left(\frac{u_{\mathrm{A}}(n)}{n}\right)^2 + \left(\frac{u_{\mathrm{B}}(n)}{n}\right)^2 \tag{70}$$

The type A terms are already defined by Eqs. (43) and (44). They vary directly as the root-mean-square value of χ, which itself depends particularly on the current source noise. Since the current noise is randomly distributed, both type A terms do not depend on time. The type B terms account for time-dependent systematic voltage deviations, as governed by Eqs. (5) and (45). From a formal point of view, the relevant superscripts of both expressions, W, R, P, V, and T, are now replaced by an index J for the subsequent summation:

$$u_{\mathrm{B}}^2(m) = \sum_J u_J^2(m) \tag{71}$$

$$u_{\mathrm{B}}^2(n) = \sum_J u_J^2(n) \tag{72}$$

Here $J = 3$, for example, indicates deviations caused by the error P (nonconstant power supply). Using Eqs. (26) and (27), respectively, the standard uncertainties of m and n can be written as follows:

$$u_J(m) = \frac{\sum t_i' \sum \delta U_i^{\mathrm{J}} - N \sum t_i' \, \delta U_i^{\mathrm{J}}}{(\sum t_i')^2 - N \sum t_i'^2} \tag{73}$$

$$u_J(n) = \frac{1}{N} \left(\sum \delta U_i^{\mathrm{J}} - u_j(m) \sum t_i' \right) \tag{74}$$

These equations now complete the set of expressions that are necessary for the assessment of the standard uncertainty of the linear THS method.

5. RESULTS

First, theoretical values for the standard uncertainty in the thermal conductivity of a Pyrex reference are calculated for the nonlinear and linear methods. The results are presented side by side in tables for a more convenient comparison. Second, they are validated by experimental data.

5.1. Theoretical Values

Two typical solutions to Eq. (29) for the nonlinear and linear evaluation procedures have been derived. The parameters of a Pyrex CRM 039 (Certified Reference Material) sample are listed in Table I.

The values for "strip width" and "evaluation time interval" assumed here differ for the nonlinear (NL) and the linear (L) procedure. Both

Table I. Experimental Parameters of a Measurement on Pyrex CRM 039 (See Text)

Thermal conductivity	$1.14\ \mathrm{W \cdot m^{-1} \cdot K^{-1}}$
Thermal diffusivity	$0.5\ \mathrm{mm^2 \cdot s^{-1}}$
Working temperature	23°C
Rate of heat flow	0.4 W
Strip length	100 ± 0.5 mm
Strip width (NL)[a]	5 ± 0.05 mm
Strip width (L)[a]	1 ± 0.05 mm
Strip thickness	0.01 mm
Strip heat capacity	$450\ \mathrm{J \cdot kg^{-1} \cdot K^{-1}}$
Strip density	$9000\ \mathrm{kg \cdot m^{-3}}$
Strip temperature coefficient	$0.006 \pm 0.00005\ \mathrm{K^{-1}}$
Evaluation time interval (NL)	[1.2, 40] s
Evaluation time interval (L)	[2.0, 40] s
Max. temperature excursion	1.9 K
Sampling rate	$14.3\ \mathrm{s^{-1}}$
Current	1 ± 0.007 A
Voltmeter uncertainty	4×10^{-5} V
Voltmeter integration time	0.017 s
Sample thickness	30 mm
Temperature drift	$1 \times 10^{-4}\ \mathrm{K \cdot s^{-1}}$

[a] NL, nonlinear; L, linear.

modifications are necessary in order to assess the uncertainty for optimum experiment parameters that are different for both procedures.

First, the type B variances, $u^2_{\mathrm{B(J)}}$, of parameters $k(\lambda)$ and a of the nonlinear model and parameters $m(\lambda)$ and $n(\lambda, a)$ of the linear method are determined. These variances depend on certain model errors, "J," as introduced by Eqs. (5) and (45). The results, being obtained from Eqs. (65) and (66) and Eqs. (73) and (74), respectively, are given in Table II. In order to identify the different variances for the nonlinear and linear models, subsequently they are denoted by superscripts "NL" and "L," respectively. Second, the type A variances for measurands λ and a from input quantities x_i and evaluation errors are calculated for both methods. They are listed in Table III. Including all the values into the related equations as given in Sections 4.1. and 4.2, one, first, obtains the relative standard deviation of λ and a in percentage for the nonlinear and linear methods:

$$u^{\mathrm{NL}}(\lambda)/\lambda = 2.6\,\%, \qquad u^{\mathrm{L}}(\lambda)/\lambda = 2.5\,\%$$

$$u^{\mathrm{NL}}(a)/a = 11\,\%, \qquad u^{\mathrm{L}}(a)/a = 11\,\%$$

Table II. Type B Variances for Parameters k and a of the Nonlinear (NL) Method and Parameters m and n of the Linear (L) Method as Introduced by Model Errors (see Text)

Error "J"	$(u^{\mathrm{NL}}_{\mathrm{B(J)}}(k)/k)^2$	$(u^{\mathrm{NL}}_{\mathrm{B(J)}}(a)/a)^2$	$(u^{\mathrm{L}}_{\mathrm{B(J)}}(m)/m)^2$	$(u^{\mathrm{L}}_{\mathrm{B(J)}}(n)/n)^2$
W	6.8×10^{-6}	5.5×10^{-5}	7.6×10^{-6}	1.0×10^{-5}
R	2.6×10^{-4}	8.3×10^{-3}	1.6×10^{-5}	6.1×10^{-6}
P	1.4×10^{-4}	6.3×10^{-4}	3.4×10^{-4}	8.0×10^{-6}
V	$<10^{-8}$	1.4×10^{-6}	4.6×10^{-6}	5.6×10^{-6}
T	1.2×10^{-4}	1.4×10^{-3}	2.4×10^{-5}	3.7×10^{-6}

Finally, the relative uncertainties for a coverage factor of 2 are

$$u'^{\mathrm{NL}}(\lambda)/\lambda = 5.2\,\%, \qquad u'^{\mathrm{L}}(\lambda)/\lambda = 5\,\%$$
$$u'^{\mathrm{NL}}(a)/a = 22\,\%, \qquad u'^{\mathrm{L}}(a)/a = 22\,\%$$

5.2. Experimental Values

In order to verify the theoretical results obtained for the standard uncertainty of the thermal conductivity of the nonlinear and linear THS methods, measurements on Pyrex 7740 glass were carried out. This material, manufactured by la Société Corning France, was chosen for several reasons. Its thermal conductivity of 1.14 $\mathrm{W\cdot m^{-1}\cdot K^{-1}}$ at room temperature is representative of a wide range of dielectrics. This material has been in use for a long time and has been studied thoroughly, for example, in Refs. 9–12. Our sample has been cut from the original bulk that was used for the certification as the BCR standard reference material CRM 039 for thermal

Table III. Type A Variances for Measurands λ and a from Input Quantities x_i and Evaluation Errors (See Text) for the Nonlinear (NL) and Linear (L) Methods

Input quantity x_i	$(u^{\mathrm{NL}}_{xi}(\lambda)/\lambda)^2$	$(u^{\mathrm{NL}}_{xi}(a)/a)^2$	$(u^{\mathrm{L}}_{xi}(\lambda)/\lambda)^2$	$(u^{\mathrm{L}}_{xi}(a)/a)^2$
α	7×10^{-5}	—	7×10^{-5}	—
U_0	1×10^{-8}	—	1×10^{-8}	—
I	5×10^{-5}	—	5×10^{-5}	—
L	2.5×10^{-5}	—	2.5×10^{-5}	—
D	—	1.0×10^{-4}	—	2.5×10^{-3}
m	—	—	3.8×10^{-4}	3.9×10^{-3}
n	—	—	—	3.5×10^{-4}
Evaluation Error	2.8×10^{-5}	1.6×10^{-3}	1.1×10^{-4}	5×10^{-3}

conductivity [12] in which PTB cooperated. Moreover, our IR absorption spectra on Pyrex show that, within the temperature range of the measurements, i.e., from -75 to 195 °C, there will be no significant radiative heat transfer.

The experiments were performed using a nickel strip 100 mm in length, 0.01 mm in thickness, and 3 mm in width. [A strip width of $D = 3$ mm has been chosen in order to ensure comparability of experimental data with both our analytical assessments for $D^{NL} = 5$ mm (nonlinear method) and $D^{L} = 1$ mm (linear method).] The strip is clamped between both brick-shaped sample halves, each $100 \times 30 \times 18$ mm^3. The thermal part of the setup is mounted inside an insulated container that is immersed in a thermostated bath. In a four-wire circuit the strip is connected to a constant-current source and a voltmeter. Beginning at time zero, t_0, a constant current of 1 A is passed through the strip for about 2 min while the voltage drop $U_i(t)$ is recorded pointwise at a sampling rate of 14 s^{-1}. For each working temperature T_W, three repeated runs were performed.

Each data set, $\Delta U_i(t)|_{T_W}$, was analyzed twice. First, the linear and, then, the nonlinear evaluation procedures were carried out. Both are described in some detail in Refs. 3 and 4, respectively. From the linear procedure, not only were the values of the measurands obtained, but also the practical upper end point t_{max} of each THS signal. Using this substantial information as input, the nonlinear evaluation was performed numerically, thus providing a second pair of values for thermal conductivity and thermal diffusivity.

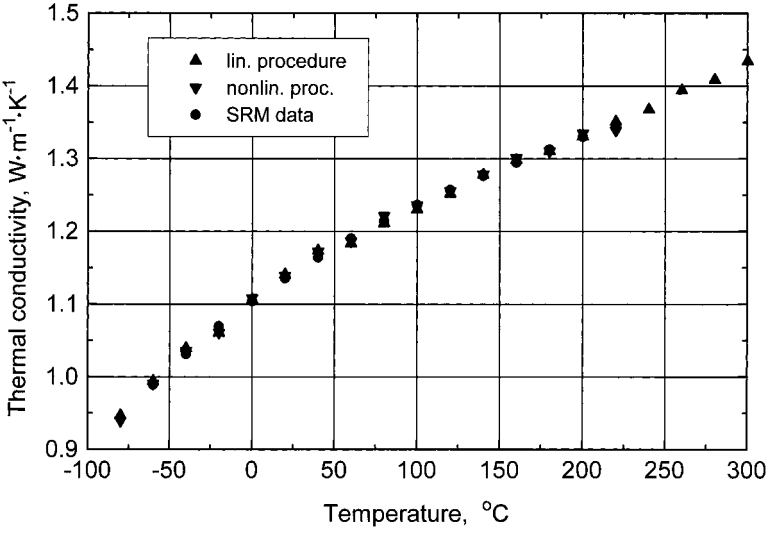

Fig. 12. Thermal conductivity of Pyrex CRM 039 vs temperature, evaluated by two mathematical models and against certified standard reference data.

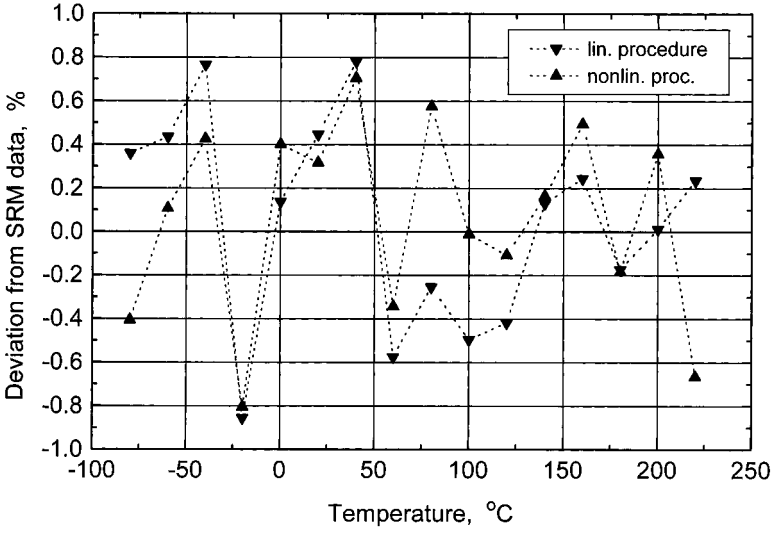

Fig. 13. Experimental data sets as shown in Fig. 12 in comparison with the certified standard data of Pyrex CRM 039 (baseline).

Figure 12 presents the results obtained by us for the thermal conductivity of Pyrex CRM 039 vs temperature along with the certified reference data (indicated as SRM data). As can be seen, the three data sets agree very well. Figure 13 shows the deviation of our two experimental data sets from the SRM data (baseline). The maximum departure is 0.8% for each data set. This value is much smaller than the estimated standard uncertainties of both the nonlinear and the linear methods. Obviously, there is no systematic difference, either between each of our data sets, on the one hand, and the reference values, on the other hand, or between our data sets themselves. Thus, the scatter in the data is due to the measurement procedure, not to data analysis.

In Ref. 12 an uncertainty of at least 1.2% is claimed for the SRM data. Hence, the uncertainty values being estimated for both the nonlinear and the linear THS methods are in good agreement. However, as mentioned above, for the nonlinear method the most significant source of systematic error, the undefined upper end point, is not considered here.

6. SUMMARY

The ISO standard uncertainties of the thermal transport poperties, λ and a, have been calculated for given values of the bcr standard reference

material CRM 039, Pyrex 7740. However, the expressions have been generalized so that the appropriate values can easily be used to examine possible errors for other dielectrics.

The assessment is made for three major classes of error sources, namely, the model error, the evaluation error, and the measurement error. The first class comprises errors due to deviations of the ideal physical model from the practical setup, the second one covers errors arising from the scatter of experimental data, and the third one comprises errors of the peripheral measurement instruments.

The error analysis is presented for the nonlinear (classical) and linearized THS models. Since the classical model is implicit, the sensitivity coefficients of the variances in the measurands cannot be calculated analytically. They must be estimated numerically using a newly developed procedure. The analysis of errors indicates that, for the nonlinear method, the precision in localizing the theoretically undefined upper end point of the time interval that is valid in practice is the major source.

The recently developed linearization transforms the complex classical model into a linear and explicit model. As a first favorable consequence, the measurands λ and a can now be determined from the slope and intercept of the linearized THS signal. The above-mentioned model error is thus no longer crucial.

As a second consequence, for the first time the explicit character of the linear method now allows the uncertainty to be assessed in complete agreement with the recommendations of the relevant ISO guide. Since the linearization of the mathematical model does not lead to any substantial increase in uncertainty, both pairs of results may be considered as equivalent to a first-order approximation and, thus, mutually comparable. For the nonlinear and linear THS methods the associated standard uncertainties of λ differ only slightly (2.6% and 2.5%), while the standard uncertainty of a is 11% for both methods. It should be pointed out that the model error of the linear THS method is considerably smaller than that of the closely related THW technique, provided that both methods are realized in the same interval of dimensionless time.

Finally, the uncertainty in λ is assessed experimentally against Pyrex as the reference standard CRM 039 for temperatures between -75 and $195\,^{\circ}$C. The deviations are within a range of $\pm 0.8\%$ and, hence, confirm the theoretical results.

REFERENCES

1. ISO, *Guide to the Expression of Uncertainty in Measurement* (1992).
2. S. E. Gustafsson, E. Karawacki, and M. N. Khan, *J. Phys. D* **12**:1411 (1979).

3. W. Sabuga and U. Hammerschmidt, *Int. J. Thermophys.* **16**:557 (1995).
4. U. Hammerschmidt, in *Proc. 24th Int. Thermal Cond. Conf., Pittsburgh, 1997*, P. S. Gaal, ed. (Technomic, Lancaster, PA, 1999).
5. E. McLaughlin and J. F. Pittman, *Phil. Trans. Roy. Soc. Lond. A* **270**:557 (1971).
6. M. A. Chohan, Thesis (Chalmers University of Technology, Göteborg, 1987).
7. S. E. Gustafsson, in *Proc. Eighth Symp. Thermophys. Props., Vol. II*, J. V. Sengers, ed. (American Society of Mechanical Engineers, New York, 1982).
8. W. H. Press, B. P. Flannery, S. A. Teukolsky, and W. T. Vetterling, in *Numerical Recipes* (Cambridge University Press, New York, 1988).
9. R. Saure and U. Hammerschmidt, *Qualifizierung des Transient-Hot-Strip-Verfahrens zur Messung der Wärmeleitfähigkeit und der Temperaturleitfähigkeit dielektrischer Festkörper*, Bericht PTB-W-45 (Physikalisch-Technische Bundesanstalt, Braunschweig, 1991).
10. T. Log and M. M. Metallinou, *Rev. Sci. Instrum.* **63**:3966 (1992).
11. Y. S. Touloukian, R. W. Powell, C. Y. Ho, and P. G. Klemens, in *Thermophysical Properties of Materials* (Plenum Press, New York, 1970), Vol. 12, p. 992.
12. I. Williams and R. E. Shawyer, Certification report for a Pyrex glass reference material for thermal conductivity between $-80\,^{\circ}$C and $200\,^{\circ}$C (CRM 039), bcr information, *Reference Materials*, Report EUR 13358 (1991).